



Research article

Structure and properties of NdCuGa₃ single crystals

Binod K. Rai^{a,*}, Boris Maiorov^b, Krzysztof Gofryk^{c,d}, Patrick O'Rourke^a, Catherine Housley^a, Henry Ajo^a, Asraf Sawon^e, Arjun K. Pathak^e, Narayan Poudel^c, Qiang Zhang^f, Travis J. Williams^f, Matthias Frontzek^f

^a Savannah River National Laboratory, Aiken, SC, 29808, USA

^b Los Alamos National Laboratory, Los Alamos, NM 87545, USA

^c Idaho National Laboratory, Idaho Falls, Idaho 83402, USA

^d Center for Quantum Actinide Science and Technology, Idaho National Laboratory, Idaho Falls, Idaho 83415, USA

^e Department of Physics, SUNY Buffalo State, Buffalo, New York 14222, USA

^f Neutron Scattering Division, Oak Ridge National Laboratory, Oak Ridge, TN 37831, USA

ARTICLE INFO

Keywords:

Antiferromagnetism
Crystal structure
Flux growth
Neutron diffraction
X-ray diffraction
Specific heat

ABSTRACT

This manuscript reports on the structural and magnetic properties of NdCuGa₃ using powder and single crystal X-ray diffraction (XRD), zero-field single crystal neutron diffraction, magnetization, and specific heat measurements. Our XRD on a single crystal specimen of NdCuGa₃ confirmed that it crystallizes in the tetragonal BaNiSi₃-type structure. A magnetic phase transition at $T_N = 3.3$ K is assessed using specific heat and magnetic susceptibility measurements. No additional anomaly below T_N down to 50 mK was detected by performing specific heat measurements. Neutron single crystal diffraction data collected at $T = 300$ mK confirm the antiferromagnetic phase below $T_N = 3.3$ K with the propagation vector $\vec{\tau} = (0.2, 0, 0)$. Possible magnetic structure solutions of NdCuGa₃ are discussed.

1. Introduction

The magnetism of rare-earth-based intermetallic compounds is attributed to the partially filled 4*f* electron shell, and such systems have shown complex but interesting physical properties such as hidden order magnetism, exotic magnetic phases, heavy-fermions, quantum criticality, unconventional superconductivity, and recently topological phases [1–12]. This is particularly true in the RTX_3 (rare earth *R*, transition metals *T* and main group element *X* of 13, 14, or 15) family, where in addition to many of the above properties vibronic bound states, valence fluctuations, metamagnetisms, and spin-glass behavior have been reported [13,14]. These systems crystallize in the BaNiSi₃-type structure, which is derived from the BaAl₄-type and is similar to ThCr₂Si₂ [13]. Interestingly, in the BaNiSi₃-type structure (space group *I4mm*), an *R*-element resides on a single crystallographic site and the structure lacks inversion symmetry [15]. That, together with the complex magnetic structures present in this family of compounds, could make it an attractive platform to search for new quantum states of matter in the RTX_3 system [15–18].

Noncentrosymmetric materials are widely recognized as potential hosts for complex magnetic textures due to competing interactions. For instance, EuRGe₃ single crystal neutron diffraction and resonant X-ray

diffraction studies reported complex magnetic structures below $T_N = 12.2$ K, $T'_N = 7.0$ K, and $T_N^* = 5.0$ K, including the cycloidal magnetic ordering below T'_N [16]. EuNiGe₃ is reported to show helimagnetic order and has been suggested to possibly show a skyrmion phase based on the anomalous Hall effect [19,20]. NdCoGe₃ is another noncentrosymmetric compound that exhibits modulated magnetic structure in zero magnetic field and complex field-induced magnetic phases [15]. Despite extensive research efforts, many interesting magnetic ground states in the RTX_3 family of compounds have yet to be discovered [13].

NdCuGa₃ is reported to crystallize in the BaNiSi₃-type tetragonal structure (*I4mm*) based on the single crystal XRD study performed on a single crystal separated from arc-melted polycrystalline ingots [21]. Subbarao et al. [21] has shown that the BaNiSi₃-type structure in NdCuGa₃ is structurally stable from 100 K to 400 K by performing the temperature-dependent single crystal XRD study. Although this study describes single crystal XRD on small pieces isolated from arc-melted polycrystalline ingots, such analyses on as-grown single crystals have yet to be reported.

Nakalashmi et al. [22] reported on magnetic properties of single crystalline NdCuGa₃ with a long-range antiferromagnetic (AFM) order below an Néel temperature of $T_N = 3.3$ K, and suggested a complex

* Corresponding author.

E-mail address: binod.raai@srnl.doe.gov (B.K. Rai).

nature of magnetic ordering. Moreover, muon spin rotation/relaxation (μ SR) measurements performed on polycrystalline NdCuGa₃ suggested an incommensurate magnetic order below T_N [23]. The knowledge of the magnetic ground state of the compounds is best gained using neutron diffraction together with detailed thermodynamic properties under an applied magnetic field, which is currently lacking for NdCuGa₃.

Here we report the structural and magnetic properties of NdCuGa₃ using powder and single crystal X-ray diffraction, single crystal neutron diffraction, ac and DC magnetic susceptibility, and specific heat measurements. Our single crystal XRD on a single crystal species confirmed that NdCuGa₃ crystallizes in the tetragonal BaNiSi₃-type structure. We performed low-temperature specific heat characterizations down to 50 mK and detected only one bulk phase transition around 3.3 K, corresponding to antiferromagnetic ordering. Neutron single crystal diffraction data confirmed the antiferromagnetic phase below $T_N = 3.3$ K and no additional phase transition down to 300 mK. The neutron data can be modeled with a sine-modulated structure with a propagation vector $\vec{\tau} = (0.2, 0, 0)$ with a magnetic moment parallel to the propagation vector. This model is supported by the information in the bulk magnetic properties.

2. Methods

Single crystals of NdCuGa₃ were synthesized using a self-flux technique similar to that previously used to grow NdCoGe₃ [15]. Nd, Cu, and Ge elements were placed in Al₂O₃ Canfield crucible sets [24] in the molar ratio Nd:Cu:Ga = 10:15:75 and sealed in silica ampoules under 1/3 atm of Ar. The ampoules were heated to 1060 °C and held for 6 h, cooled to 620 °C over 70 h, and then the ampoules were removed from the furnace, and the crystals were separated from the flux using a centrifuge. The as-grown single crystals were subsequently annealed for 80 h under a partial Ar atmosphere at 800 °C.

The phase purity and crystal structure of the NdCuGa₃ were examined by room temperature X-ray powder diffraction using a PANalytical X'Pert Pro MPD diffractometer with monochromatic Cu $K_{\alpha 1}$. Single-Crystal XRD data on the annealed crystal at 300 K were collected using a Rigaku XtaLAB Synergy-S X-ray diffractometer equipped with a Mo-target ($\lambda = 0.71073$ Å) and a HyPix-6000HE hybrid photon counting (HPC) detector, operating at 50 kV and 1 mA. To ensure completeness and desired redundancy, the CrysAlisPro program was used for data collection strategy, data collection, and processing [25]. The structure was solved via intrinsic phasing methods using ShelXT and refined using ShelXL in the Olex2 graphical user interface [26–28]. Crystallographic data can be found in Tables 1. Anisotropic magnetization and specific heat measurements were performed in a Quantum Design Dynacool Physical Property Measurement System (PPMS).

The single crystal of NdCuGa₃ (mass = 45 mg) was glued on a thin Cu-sheet with Ge-varnish in $HK0$ scattering geometry; the sheet was then mounted on a Cu-clamp holder, which was screwed into the mounting of the Heliox-7 ACV. The Heliox-7 ACV is a closed-cycle, one-shot ³He refrigerator with a high-power CCR for cooling capable of providing a base temperature of 300 mK for 48 h. The neutron scattering experiment was performed at the WAND² diffractometer at the High-Flux-Isotope reactor at Oak Ridge National Laboratory. Data were collected in 0.1° steps over 180° with a count time of 38 s per step. The detector was lifted to simultaneously collect $HK0$ and $HK1$ maps. The wavelength was 1.486 Å. The data were reduced using Mantid [29]. The data were corrected for detector efficiency with a vanadium measurement, and the surrounding background of the reflections was subtracted from the integration over the whole reflection. Symmetry analysis was performed using SARA [30], and the Rietveld refinement of the magnetic structure was done in FullProf [31].

Table 1

Crystallographic Data for NdCuGa₃ at $T = 300$ K (Wavelength = 0.71073 Å, Crystallographic System = Tetragonal, space group = $I4mm$, $Z = 2$)

a (Å)	4.21380(10)
b (Å)	4.21380(10)
c (Å)	10.5060(2)
Volume (Å ³)	186.546(10)
Density (g/cm ⁻³)	7.422
Absorption coefficient	40.394
Crystal dimensions (mm ³)	0.11×0.08×0.05
θ range (Å)	3.879–30.937
Measured reflections	1965
Independent reflections	209
R_{int}	0.041
Goodness of fit	1.22
Final R indices [$> 2\sigma(I)$]	$R_1 = 0.0166$ $wR_1 = 0.036$
Largest diff. peak and hole (Å ⁻³)	0.42 and -0.62

$$^a R_1 = \sum ||F_o| - |F_c|| / \sum |F_o|$$

$$^b wR_2 = [\sum [w(F_o^2 - F_c^2)^2] / \sum [w(F_o^2)^2]]^{1/2}.$$

Table 2

Atomic positions, Occupancies, and U_{eq} values for NdCuGa₃ at room temperature.

Atoms	x	y	z	Occupancy	U_{eq} (Å ²)
Nd	0	0	0.6144(4)	1	0.0074(2)
Cu	0	0	0.2263(12)	1	0.0141(11)
Ga1	0	0	0.0000	1	80.0112(8)
Ga2	0	0.5	0.3646(6)	1	0.0112(3)

3. Results

3.1. Crystal structure

The single crystal XRD data were collected on high-quality NdCuGa₃ crystals at room temperature. The solved crystal structure revealed a non-centrosymmetric BaNiSn₃-type ($I4mm$ space group) with full atomic occupancy, in agreement with literature [21]. In this structure type, T and X atoms occupy different Wyckoff sites (Cu atom at $2a$ site and two Ga atoms at $4b$ and $2a$ sites), distinct from the closely related centrosymmetric ThCr₂Si₂-type ($I4/mmm$ space group) structures where T and X atoms share the Wyckoff site $4e$ (one Ga atom at $4d$ site and Cu/Ga mixing at $4e$ site) [13,21].

In a previous study of single crystal XRD using pieces from polycrystalline ingots [21], the largest peak and deepest hole in NdCuGa₃ were quite large at 6.385 and -14.264 e/Å³, respectively at 300 K. However, in the current study the largest peak and the deepest hole were 0.42 and -0.62 e/Å³ at 300 K, similar to 200 K and 400 K values in Subbarao et al. [21]. The refined lattice parameters in space group $I4mm$ are $a = 4.2138(10)$ Å and $c = 10.5060(2)$ Å with R_1 , wR_1 and χ^2 of 2%, 4.6% and 1.1%. These R_1 , wR_1 , and χ^2 parameters are also much smaller than in the previous study [21], indicating perhaps that the quality of single crystals obtained from the flux-growth is better than that of single crystals extracted from arc-melted polycrystalline ingots. The other crystal structure information is provided in Table 1 (see Table 2).

The phase purity and crystal quality of the NdCuGa₃ single crystals were also verified by powder X-ray diffraction at room temperature on a pulverized crystal. The collected powder diffraction is indexed and analyzed using the crystallographic information file (CIF) generated from single crystal XRD diffraction (see Fig. 1). The XRD pattern analysis is performed with the Fullprof program using the Rietveld technique. The refined lattice parameters at room temperature are $a = 4.210(3)$ Å and $c = 10.489(97)$ Å with the goodness of fit 1.41.

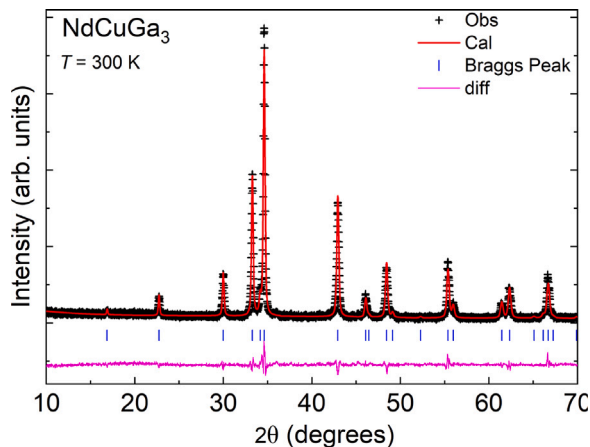


Fig. 1. Room-temperature X-ray powder diffraction pattern of NdCuGa₃ for a pulverized crystal (symbol) together with the Rietveld refinement (red line) and Bragg positions (vertical lines).

3.2. Magnetic properties

Magnetization data for NdCuGa₃ are shown in Fig. 2. NdCuGa₃ shows anisotropic behavior as observed in the temperature-dependent magnetization. The high-temperature magnetization (150–350 K) displays Curie–Weiss behavior, as shown in Fig. 2(a). The effective moment $\mu_{eff} = 3.62 \mu_B/\text{Nd}$ and Weiss temperatures $\theta_{W,ab} = 25 \text{ K}$ and $\theta_{W,c} = -29 \text{ K}$ are extracted from the Curie–Weiss fit of the inverse magnetic susceptibility ($1/\chi = H/M$). The obtained effective moment is the same as expected for Nd³⁺ ion calculated under $L - S$, Russell–Saunders coupling approximation. The isothermal magnetization $M(H)$ of NdCuGa₃ also shows anisotropic magnetization, as shown in Fig. 2(b). The magnetization is larger for $H \perp c$ than for $H//c$, consistent with the temperature-dependent $M/H(T)$ and $M(H)$ data are consistent with the literature and reveal easy-plane anisotropy. Furthermore, $M(H)$ shows the non-linear magnetic response to the applied magnetic field $H \perp c$, with a metamagnetic-like transition $\mu_0 H \approx 0.6 \text{ T}$ at $T = 2 \text{ K}$ and induced magnetic moment $2.1 \mu_B/\text{Nd}$ at $\mu_0 H = 6 \text{ T}$. This value is close to the $2.2 \mu_B/\text{Nd}$ measured for elemental Nd metal [32].

We now turn to understand the magnetic response when the field is applied along the tetragonal plane, $H \perp c$, where the non-linear magnetic response in $M(H)$ exists. To investigate the non-linear magnetic response to the applied field $H \perp c$, the low-temperature and low-field magnetization data are measured as in grown and annealed crystals (see Fig. 3). In both crystals, the low-temperature magnetization with an applied field $H//ab$ shows an upturn in magnetization well above $T_N = 3.3 \text{ K}$ on lowering the temperature. The overall low-temperature magnetization decreases when applying a higher magnetic field, as shown in Fig. 3. The magnitude of the magnetization of the annealed crystal is higher than the as-grown crystal at low temperatures, which is the only difference between these crystals with the applied field. Thus, magnetization characterization and specific heat measurements were performed with $H \perp c$ on only annealed NdCuGa₃ single crystal. Although the upturn in the magnetization on lowering temperature is consistent with a previous study [22], its nature is unclear. Since our neutron diffraction study (discussed below) confirms the AFM ground state of NdCuGa₃, the upturn in the low-temperature magnetization could be related to some domain pinning effect which can be present in any materials with a low level of disorder [4]. Future studies are needed to draw firm conclusions on the origin of this behavior.

The magnetic phase transition temperature of NdCuGa₃ is difficult to mark in the $M/H(T)$ data due to the upturn in the temperature-dependent $M/H(T)$. Thus, we performed ac magnetic susceptibility

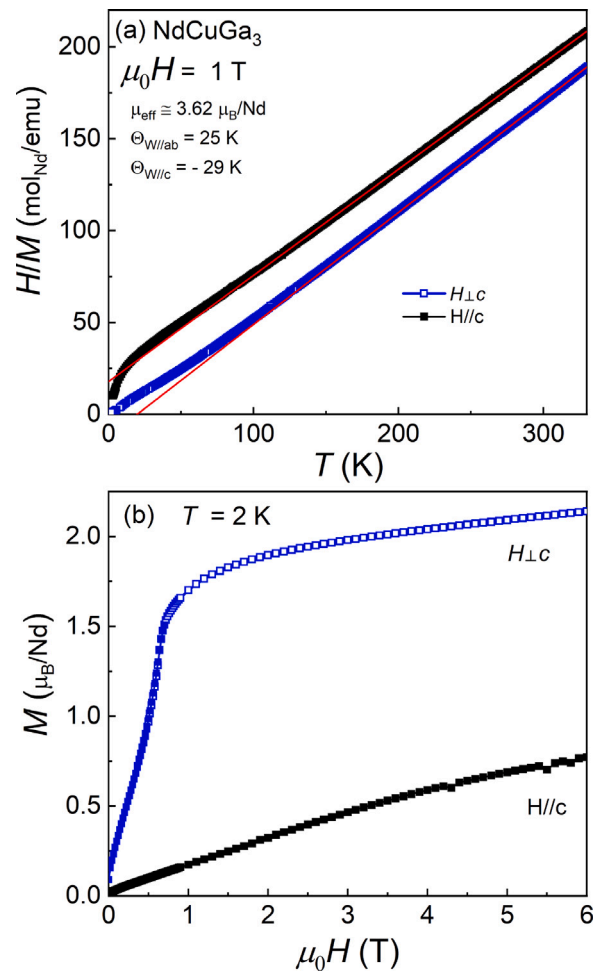


Fig. 2. The inverse magnetic susceptibility ($1/\chi = H/M$) of NdCuGa₃ for different orientations of the applied field $\mu_0 H = 1 \text{ T}$. The red line is the Curie Weiss model fitted between 150 and 350 K. (b) Anisotropic isothermal magnetization at $T = 2 \text{ K}$ of NdCuGa₃.

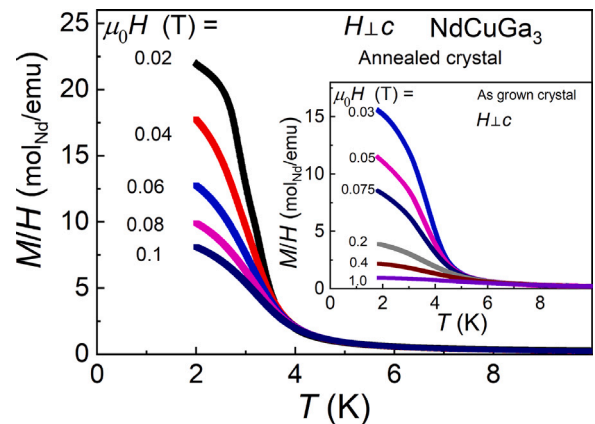


Fig. 3. The low-temperature magnetization M/H of NdCuGa₃ annealed crystals with different applied fields $H \perp c$. Inset: The low-temperature magnetization M/H of NdCuGa₃ as grown crystals with applied fields $H \perp c$.

measurements to determine the magnetic phase transitions (see Fig. 4). The in-phase contribution $\chi'(T)$ shows an anomaly at T_N , which corresponds to a dip in the $d\chi'/dT$ (see inset of Fig. 4(b)). The anomaly associated with T_N gets suppressed with the applied field and completely disappears with a 0.6 T magnetic field. The broad cusp around

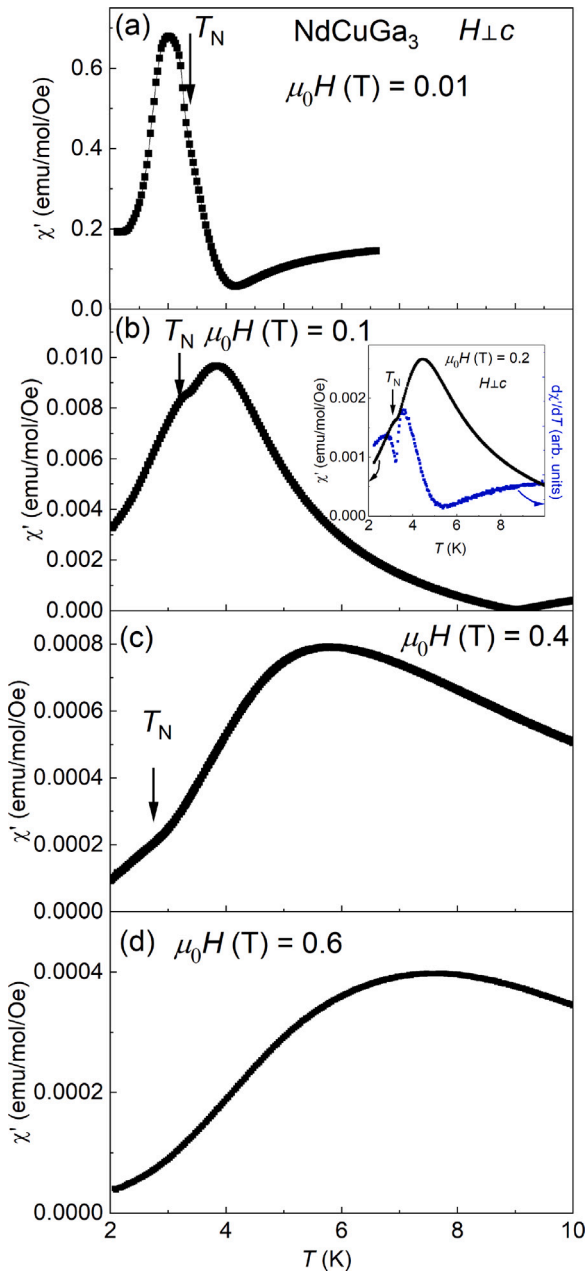


Fig. 4. The in-phase contribution χ' of ac susceptibility data at (a) $\mu_0 H = 0.01$ T, (b) $\mu_0 H = 0.1$ T and $\mu_0 H = 0.2$ T (inset), (c) $\mu_0 H = 0.4$ T, and (d) $\mu_0 H = 0.6$ T.

$T = 4\text{--}5$ K corresponds to the temperature where the upturn in the temperature-dependent $M/H(T)$ develops upon applying magnetic fields and is pushed to higher temperatures with higher fields, as shown in Fig. 4. One may suspect short-range (ferro)magnetic correlations in this temperature range. No indications for these were found in the single crystal neutron diffraction, but the associated broad magnetic diffuse scattering might be below the detection limit.

Previous studies of NdCuGa₃ did not report physical properties below $T = 2$ K [22,23]. We have performed specific heat $C_p(T)$ measurement at zero-field to determine T_N and examine any additional magnetic phase transition below 2 K (see Fig. 5). $C_p(T)$ shows a sharp anomaly around $T = 3.3$ K, consistent with the reported T_N . Furthermore, the specific heat measurement performed down to $T = 50$ mK excludes the existence of further low-temperature magnetic transition in NdCuGa₃. The inset of Fig. 5 shows the suppression of T_N

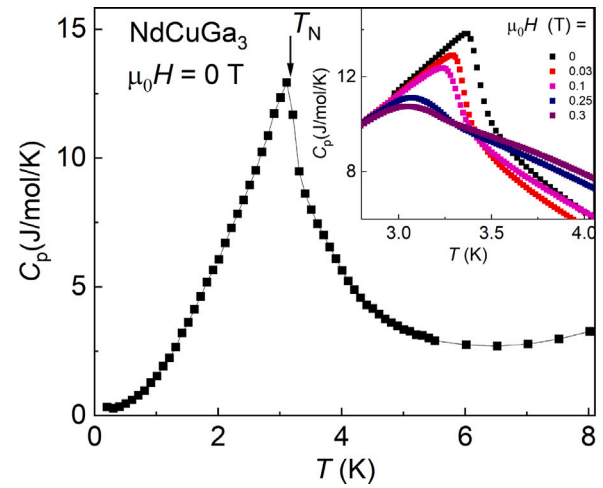


Fig. 5. Specific heat capacity C_p of NdCuGa₃ in zero applied field demonstrating anomalies at T_N . Inset shows C_p under applied magnetic fields.

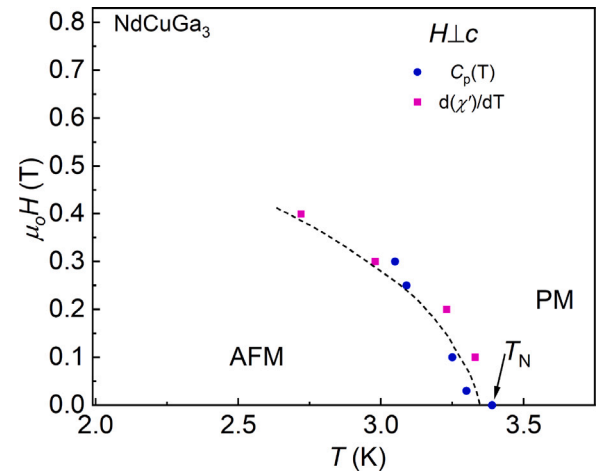


Fig. 6. The H vs. T magnetic phase diagram of NdCuGa₃ is constructed with transitions determined from specific heat and ac susceptibility data as indicated by the legend.

with applied magnetic fields $H \perp c$. However, the sample experienced a large torque with the applied magnetic field therefore, we limit it to 0.3 T. The magnetic phase diagram of NdCuGa₃ for $H \perp c$ is shown in Fig. 6. The magnetic phase diagram is constructed utilizing a peak in specific heat and a dip in the derivatives of ac-susceptibility $\chi(T)$. Based on the $\chi(T)$ data, the critical field for T_N is less than 0.6 T.

3.3. Neutron diffraction

The neutron data collected at 300 mK shows magnetic satellites around the nuclear reflections (Fig. 7(a)). These reflections are absent at 4 K (above the ordering temperature). Other observed weak, non-indexable reflections show no temperature dependence. The magnetic satellites can be indexed with a propagation vector $\tau = (0.2, 0, 0)$ with the star of the τ consisting of $\pm \tau_1 = (\pm 0.2, 0, 0)$ and $\pm \tau_2 = (0, \pm 0.2, 0)$. Only first-order magnetic reflections are observed. The overall intensity of the magnetic reflections is quite weak, for instance, the ratio of integrated intensities $I(110-\tau_1)/I(110)$ is 3.2%. The magnetic intensity has a particular Q -dependence, as shown in Fig. 7(b). Around the 031 reflection (similar for 020 and 200), only the satellites for $\pm \tau_1$ are observed, while the satellites for $\pm \tau_2$ are either absent or very faint. Recalling that the magnetic scattering is only sensitive to the perpendicular component of the magnetization, this observation

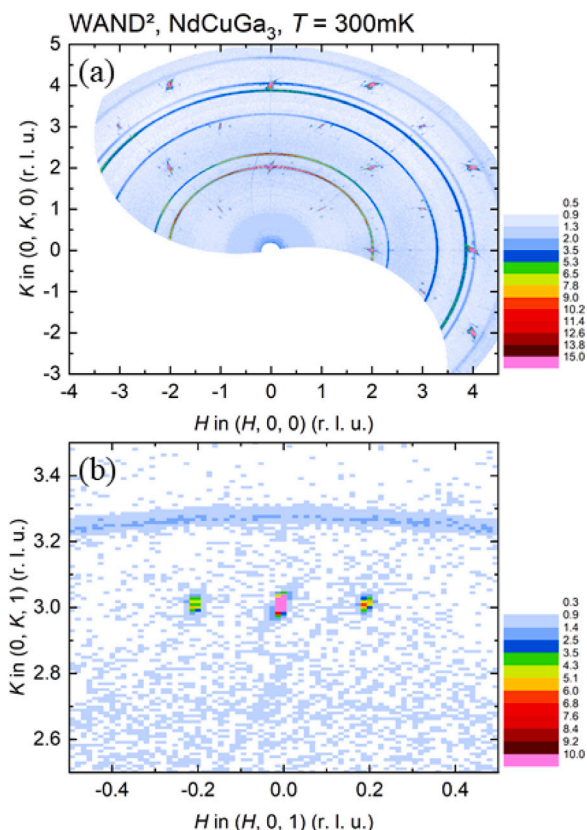


Fig. 7. (a) Reciprocal $HK0$ map of NdCuGa_3 , measured at 300 mK. Weak magnetic satellite reflections are observed in a four-fold pattern around the nuclear Bragg peaks and can be indexed by the propagation vectors τ_1 and τ_2 (see text). The powder lines originate from the Cu-sample holder. (b) Detailed view of the 031 reflections and the two clearly observed τ_1 satellites. The satellites generated by τ_2 are barely visible, indicating that the magnetic moments are parallel to the propagation vector.

indicates that the magnetic moment direction is mostly parallel to the propagation vector. Measurements of the reciprocal map have been repeated for 3 K (slightly below T_N) and 4 K (slightly above T_N). Noteworthy is that there is no observable change in the propagation vector between 3 K and 300 mK and no additional magnetic scattering, indicating only a magnetic phase below T_N .

Symmetry analysis for space group 107 ($I4mm$) using the propagation vector τ yields two irreducible representations. The first, Γ_1 yields a basis vector along the b -direction perpendicular to the propagation vector and is not considered due to the observed Q -dependence. The second irrep, Γ_2 has two basis vectors, one along the a -direction and one along the c -direction. Since a small c -component of the magnetic moment cannot be excluded from the measured data, the magnetic structure refinement varied moment components along both basis vectors without further restriction.

For the magnetic structure refinement, first the nuclear reflections from the $HK0$ and $HK1$ plane were integrated, yielding 28 reflections, of which 10 are independent. The refinement of the nuclear data used the refinement data from the X-ray measurement without isotropic or anisotropic temperature parameters. The refinement of temperature parameters was unstable due to the small number of independent reflections. Only two parameters were refined, i.e., scale and extinction. The final R_F factor was 5.58. The refinement of the magnetic structure used the scale factor divided by 2 (assuming equal domain population) and the extinction factor to refine data sets for τ_1 (35 reflections) and τ_2 (36 reflections) independently. Some of the magnetic reflections were found directly on top of the powder lines, and given the overall weak intensity, these reflections have not been included in the refinement.

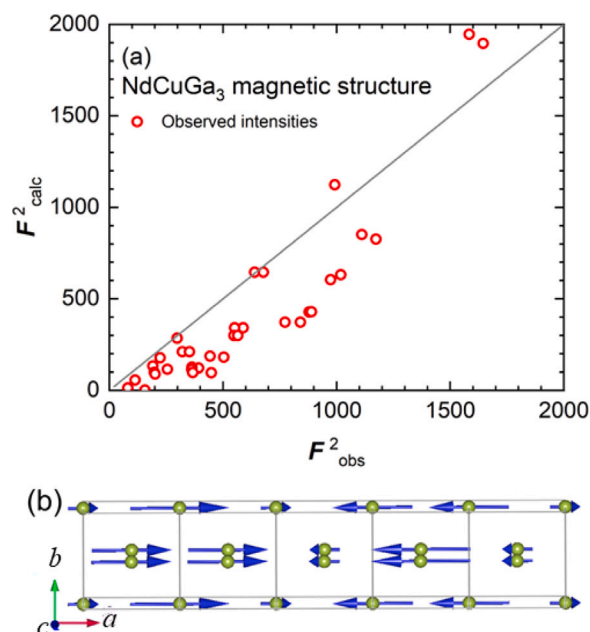


Fig. 8. (a) plot of F_{obs}^2 vs. F_{calc}^2 for the refinement of the τ_1 reflection set. (b) Sketch of the resulting magnetic structure. The magnetic moment on the positions where the arrow is too short to be displayed is $0.7 \mu_B$.

Refined parameters were the two-moment contributions along the directions of the two basis vectors. Both refinements yielded maximum magnetic moment values $2.33(7) \mu_B$ for τ_1 and $2.13 \mu_B$ for τ_2 lower than the expected value for Nd^{3+} of $3.27 \mu_B$, which however is not unexpected for a sine-modulated structure. The magnetic moment value agrees with the observed magnetic moment in the magnetization data and the observed magnetic moment in Nd-metal. The R_F factor for both refinements is relatively large with 25.

The large R_F value is partly due to the observation of the two strongest magnetic peaks, which are quite separate from the other reflections with respect to the measured intensities. Also, the smaller intensity reflections seem to have systematically slightly higher intensity. To extract integrated intensity, integration in an ellipsoid with background subtraction from an outer ellipsoid was performed. The resulting background subtraction sphere was homogeneous by visual inspection but might underestimate the “true” background under the peak. Again, the weak signal of the magnetic reflection leads to the potential emphasis of small contributions to the extracted integrated intensities. Based on the available information and data, the magnetic structure of NdCuGa_3 at 300 mK is a sine-modulated structure with a propagation vector of $(0.2, 0, 0)$ (see Fig. 8). The magnetic moment is parallel to the propagation vector. A cycloidal magnetic structure fits the data with comparable R_F values but would have a larger moment contribution along the c -direction, which would be in disagreement with the observed anisotropy in the magnetization.

In a Kramer’s doublet system with a local moment behavior of rare-earth intermetallic compounds and a lack of Kondo interaction, a modulated magnetic structure with a constant amplitude or a commensurate magnetic structure is often the expected ground state. However, recently an amplitude-modulated magnetic ground state (spin density wave) is reported in NdCoGe_3 with $\vec{\tau} = (0.494, 0.0044, 0.385)$ at 1.8 K [15]. NdCuGa_3 is an isostructural compound to NdCoGe_3 , showing a sine-modulated structure as a ground state. In NdCoGe_3 , the modulated wave vectors are in all three directions, unlike NdCuGa_3 , where the modulated wave vector is confined in the tetragonal plane. Note that no magnetic transition is observed below $T_N = 3.3$ K down to 300 mK in the single crystal neutron diffraction and 50 mK in the specific heat measurements.

3.4. Summary

In conclusion, we report the structural and magnetic properties of NdCuGa₃ using powder and single crystal X-ray diffraction, single crystal neutron diffraction, magnetization, and specific heat measurements. The crystal structure information obtained from single crystals is presented in this study and confirms that NdCuGa₃ crystallizes in the tetragonal BaNiSi₃-type structure. The magnetic measurements suggest that the antiferromagnetic ground state is suppressed by the applied magnetic field ($\mu_0 H = 0.6$ T), but a short-range (ferro)magnetic correlations are developed upon higher applied magnetic fields. Neutron single crystal diffraction study reveals the antiferromagnetic phase below $T_N = 3.3$ K with the propagation vector $\vec{\tau} = (0.2, 0, 0)$ and suggests a sine-modulated structure.

CRediT authorship contribution statement

Binod K. Rai: Conceived the project, Synthesized crystals, Characterized crystals, Wrote manuscript with input from all authors. **Boris Maiorov:** Characterized crystals. **Krzysztof Gofryk:** Characterized crystals. **Patrick O'Rourke:** Characterized crystals. **Catherine Housley:** Characterized crystals. **Henry Ajo:** Characterized crystals. **Asraf Sawon:** Synthesized crystals. **Arjun K. Pathak:** Synthesized crystals. **Narayan Poudel:** Characterized crystals. **Qiang Zhang:** Assisted with neutron diffraction experiment and analysis. **Travis J. Williams:** Assisted with neutron diffraction experiment and analysis. **Matthias Frontzek:** Assisted with neutron diffraction experiment and analysis, Wrote manuscript with input from all authors.

Declaration of competing interest

The authors declare that they have no known competing financial interests or personal relationships that could have appeared to influence the work reported in this paper.

Data availability

Data will be made available on request.

Acknowledgments

We thank Alex Bretaña, Gergory Morrison, and Rose Gyeer for useful discussions. We are also thankful to E. Morosan and S. Lei for the specific heat data below 2 K. This work was supported by the Laboratory Directed Research and Development (LDRD) program within the Savannah River National Laboratory (SRNL). K. G. acknowledges the U.S. Department of Energy Office of Science, Basic Energy Sciences, Physical Behavior of Materials program. A portion of this work was performed at the National High Magnetic Field Laboratory, which is supported by National Science Foundation Cooperative Agreement No. DMR-2128556*, the State of Florida, and the U.S. Department of Energy. A portion of this research used resources at the High Flux Isotope Reactor, a DOE Office of Science User Facility operated by the Oak Ridge National Laboratory. A.K.P. acknowledges the funding support from National Science Foundation, Launching Early-Career Academic Pathways in the Mathematical and Physical Sciences (LEAPS-MPS) program under Award No. DMR-2213412. This work was produced by Battelle Savannah River Alliance, LLC under Contract No. 89303321CEM000080 with the U.S. Department of Energy. Publisher acknowledges the U.S. Government license to provide public access under the DOE Public Access Plan (<http://energy.gov/downloads/doe-public-access-plan>)

References

- [1] T. Park, F. Ronning, H. Yuan, M. Salamon, R. Movshovich, J. Sarrao, J. Thompson, Hidden magnetism and quantum criticality in the heavy fermion superconductor CeRhIn₅, *Nature* 440 (7080) (2006) 65–68.
- [2] T. Kurumaji, T. Nakajima, M. Hirschberger, A. Kikkawa, Y. Yamasaki, H. Sagayama, H. Nakao, Y. Taguchi, T.-h. Arima, Y. Tokura, Skyrmion lattice with a giant topological Hall effect in a frustrated triangular-lattice magnet, *Science* 365 (6456) (2019) 914–918.
- [3] J.-X. Yin, W. Ma, T.A. Cochran, X. Xu, S.S. Zhang, H.-J. Tien, N. Shumiya, G. Cheng, K. Jiang, B. Lian, et al., Quantum-limit Chern topological magnetism in TbMn₆Sn₆, *Nature* 583 (7817) (2020) 533–536.
- [4] B.K. Rai, S. Chikara, X. Ding, I.W. Oswald, R. Schönemann, V. Loganathan, A. Hallas, H. Cao, M. Stavinoha, T. Chen, et al., Anomalous metamagnetism in the low carrier density kondo lattice YbRh₃Si₇, *Phys. Rev. X* 8 (4) (2018) 041047.
- [5] P. Gegenwart, Q. Si, F. Steglich, Quantum criticality in heavy-fermion metals, *Nat. Phys.* 4 (3) (2008) 186–197.
- [6] S. Chadov, X. Qi, J. Kübler, G.H. Fecher, C. Felser, S.C. Zhang, Tunable multifunctional topological insulators in ternary Heusler compounds, *Nat. Mater.* 9 (7) (2010) 541–545.
- [7] G. Sala, M.B. Stone, B.K. Rai, A.F. May, D.S. Parker, G.B. Halász, Y. Cheng, G. Ehlers, V.O. Garlea, Q. Zhang, et al., Crystal field splitting, local anisotropy, and low-energy excitations in the quantum magnet YbCl₃, *Phys. Rev. B* 100 (18) (2019) 180406.
- [8] B.K. Rai, M. Stavinoha, J. Banda, D. Hafner, K.A. Benavides, D. Sokolov, J.Y. Chan, M. Brando, C.-L. Huang, E. Morosan, Ferromagnetic ordering along the hard axis in the Kondo lattice YbIr₂Ge₃, *Phys. Rev. B* 99 (12) (2019) 121109.
- [9] T. Shang, R. Baumbach, K. Gofryk, F. Ronning, Z. Weng, J. Zhang, X. Lu, E. Bauer, J. Thompson, H. Yuan, CeIrIn₅: Superconductivity on a magnetic instability, *Phys. Rev. B* 89 (4) (2014) 041101.
- [10] S. Kirchner, S. Paschen, Q. Chen, S. Wirth, D. Feng, J.D. Thompson, Q. Si, Colloquium: Heavy-electron quantum criticality and single-particle spectroscopy, *Rev. Modern Phys.* 92 (1) (2020) 011002.
- [11] A. Hallas, C. Huang, B.K. Rai, A. Weiland, G.T. McCandless, J.Y. Chan, J. Beare, G. Luke, E. Morosan, Complex transport and magnetism in inhomogeneous mixed valence Ce₃Ir₄Ge₁₃, *Phys. Rev. Mater.* 3 (11) (2019) 114407.
- [12] S. Paschen, Q. Si, Quantum phases driven by strong correlations, *Nat. Rev. Phys.* 3 (1) (2021) 9–26.
- [13] B.K. Rai, P. O'Rourke, U.N. Roy, Review on crystal structures and magnetic properties of RTX₃ materials, *J. Phys.: Condens. Matter* 34 (27) (2022) 273002.
- [14] A. Kumar Singh, S. Sarkar, S.C. Peter, Diversity in crystal structure and physical properties of RETX₃ (RE=rare earth, T=transition metal, X=main group element) intermetallics, *Chem. Rec.* 22 (5) (2022) e202100317.
- [15] B.K. Rai, G. Pokharel, H.S. Arachchige, S.-H. Do, Q. Zhang, M. Matsuda, M. Frontzek, G. Sala, V.O. Garlea, A.D. Christianson, et al., Complex magnetic phases in the polar tetragonal intermetallic NdCoGe₃, *Phys. Rev. B* 103 (1) (2021) 014426.
- [16] T. Matsumura, M. Tsukagoshi, Y. Ueda, N. Higa, A. Nakao, K. Kaneko, M. Kakihana, M. Hedo, T. Nakama, Y. Ōnuki, Cycloidal magnetic ordering in noncentrosymmetric EuIrGe₃, *J. Phys. Soc. Japan* 91 (7) (2022) 073703.
- [17] P. Čermák, A. Schneidewind, B. Liu, M.M. Koza, C. Franz, R. Schönmann, O. Sobolev, C. Pfleiderer, Magnetoelastic hybrid excitations in CeAuAl₃, *Proc. Natl. Acad. Sci.* 116 (14) (2019) 6695–6700.
- [18] D. Adroja, A. del Moral, C. de la Fuente, A. Fraile, E. Goremychkin, J. Taylor, A. Hillier, F. Fernandez-Alonso, Vibron quasibound state in the noncentrosymmetric tetragonal heavy-Fermion compound CeCuAl₃, *Phys. Rev. Lett.* 108 (21) (2012) 216402.
- [19] D. Ryan, J. Cadogan, R. Rejali, C. Boyer, Complex incommensurate helicoidal magnetic ordering of EuNiGe₃, *J. Phys.: Condens. Matter* 28 (26) (2016) 266001.
- [20] W. Iha, S. Matsuda, M. Kakihana, D. Aoki, A. Nakamura, M. Nakashima, Y. Amako, T. Takeuchi, M. Kimata, Y. Otani, et al., Anomalous hall effect in antiferromagnet EuNiGe₃ with the rashba-type tetragonal structure, in: *Proceedings of the International Conference on Strongly Correlated Electron Systems, SCES2019*, 2020, 011092.
- [21] U. Subbarao, S. Rayaprol, R. Dally, M.J. Graf, S.C. Peter, Swinging symmetry, multiple structural phase transitions, and versatile physical properties in RE CuGa₃ (RE=La–Nd, Sm–Gd), *Inorganic Chem.* 55 (2) (2016) 666–675.
- [22] R. Nagalakshmi, R. Kulkarni, S. Dhar, A. Thamizhavel, V. Krishnakumar, M. Reiffers, I. Čurlík, H. Hagemann, D. Lovy, S. Nallamuthu, Magnetic properties of the tetragonal RCuGa₃ (R=Pr, Nd and Gd) single crystals, *J. Magn. Magn. Mater.* 386 (2015) 37–43.
- [23] M. Graf, J. Hettinger, K. Nemeth, R. Dally, C. Baines, U. Subbarao, S. Peter, Evolution of magnetism in LnCuGa₃ (Ln = La–Nd, Sm–Gd) studied via μ SR and specific heat, *J. Magn. Magn. Mater.* 444 (2017) 236–242.

- [24] P.C. Canfield, T. Kong, U.S. Kaluarachchi, N.H. Jo, Use of frit-disc crucibles for routine and exploratory solution growth of single crystalline samples, *Phil. Mag.* 96 (1) (2016) 84–92.
- [25] Oxford Diffraction, CrysAlisPro Software System, Rigaku Corporation Oxford, UK, 2015.
- [26] G.M. Sheldrick, Crystal structure refinement with SHELXL, *Acta Crystallogr. C* 71 (1) (2015) 3–8.
- [27] G.M. Sheldrick, SHELXT—Integrated space-group and crystal-structure determination, *Acta Crystallogr. A* 71 (1) (2015) 3–8.
- [28] O.V. Dolomanov, L.J. Bourhis, R.J. Gildea, J.A. Howard, H. Puschmann, OLEX2: a complete structure solution, refinement and analysis program, *J. Appl. Crystallogr.* 42 (2) (2009) 339–341.
- [29] O. Arnold, J.-C. Bilheux, J. Borreguero, A. Buts, S.I. Campbell, L. Chapon, M. Doucet, N. Draper, R.F. Leal, M. Gigg, et al., Mantid—Data analysis and visualization package for neutron scattering and μ SR experiments, *Nucl. Instrum. Methods Phys. Res. A* 764 (2014) 156–166.
- [30] A. Wills, A new protocol for the determination of magnetic structures using simulated annealing and representational analysis (SARAh), *Physica B* 276 (2000) 680–681.
- [31] J. Rodríguez-Carvajal, Recent advances in magnetic structure determination by neutron powder diffraction, *Physica B* 192 (1–2) (1993) 55–69.
- [32] J. Jensen, A.R. Mackintosh, *Rare Earth Magnetism*, Clarendon Press Oxford, 1991.